



Novel visible light-induced $\text{g-C}_3\text{N}_4/\text{Bi}_2\text{WO}_6$ composite photocatalysts for efficient degradation of methyl orange

Lei Ge*, Changcun Han, Jing Liu

Department of Materials Science and Engineering, College of Science, China University of Petroleum Beijing, No. 18 Fuxue Rd, Beijing 102249, PR China

ARTICLE INFO

Article history:

Received 31 May 2011

Received in revised form 12 August 2011

Accepted 12 August 2011

Available online 19 August 2011

Keywords:

$\text{g-C}_3\text{N}_4$

Bi_2WO_6

Photocatalysis

Functional

Semiconductors

ABSTRACT

Novel visible light-induced $\text{g-C}_3\text{N}_4/\text{Bi}_2\text{WO}_6$ composite photocatalysts were synthesized by introducing polymeric $\text{g-C}_3\text{N}_4$. The obtained $\text{g-C}_3\text{N}_4/\text{Bi}_2\text{WO}_6$ products were characterized by X-ray diffraction, scanning electron microscopy, transmission electron microscopy, high-resolution transmission electron microscopy, ultraviolet-visible diffuse reflection spectroscopy (DRS), and photoluminescence spectroscopy. The DRS results revealed that the $\text{g-C}_3\text{N}_4/\text{Bi}_2\text{WO}_6$ samples had a red shift and strong absorption in the visible light region. The photocatalytic oxidation ability of the novel photocatalyst was evaluated using methyl orange as a target pollutant. The photocatalysts exhibited a significantly enhanced photocatalytic performance in degrading methyl orange. The optimal $\text{g-C}_3\text{N}_4$ content for the photocatalytic activity of the heterojunction structures was determined. The synergic effect between $\text{g-C}_3\text{N}_4$ and Bi_2WO_6 was found to lead to an improved photo-generated carrier separation. Consequently, the photocatalytic performance of the $\text{g-C}_3\text{N}_4/\text{Bi}_2\text{WO}_6$ composites under visible light irradiation ($\lambda > 420 \text{ nm}$) was enhanced. The possible photocatalytic mechanism of the composites was proposed to guide the further improvement of their photocatalytic activity.

© 2011 Elsevier B.V. All rights reserved.

1. Introduction

Photocatalysis using semiconductors has received considerable interest. This process enables pollutant decomposition and hydrogen evolution via the generation of $\cdot\text{OH}$ radicals and other oxidative species [1–3]. The semiconductor TiO_2 is considered as one of the best photocatalysts [4]. However, the light response range and the photo-efficiency of TiO_2 are limited because of its wide band gap (3.2 eV) [5]. Therefore, the creation of simple, efficient, and sustainable photocatalysts that work well with visible light is a major challenge in this research field [6]. Recently, various multi-component oxide, sulfide, oxynitride, and polymer semiconductor photocatalysts have been developed for degrading organic pollutants or splitting water. Such photocatalysts include BiVO_4 [7], CdS [8], Bi_2WO_6 [9], $\text{g-C}_3\text{N}_4$ [10], BiFeO_3 [11], etc. They all exhibit activity in the photocatalytic decomposition of organics and water splitting under visible light irradiation. However, these materials have several limitations. For example, their small specific surface areas limit the improvement of their photocatalytic activities. The rapid recombination rate of their photo-generated charge carriers also seriously influences their photocatalytic efficiency.

Recently, numerous Aurivillius-based compounds have been reported to exhibit interesting photocatalytic activities. Among these compounds, Bi_2WO_6 is one of the most studied. It has attracted a great deal of attention because of its good photocatalytic activity in decomposing organic pollutants under visible light irradiation [12–16]. Several methods have been developed to prepare Bi_2WO_6 photocatalysts, such as solid-state [17], sol–gel [18], and hydrothermal [19] reactions, etc. However, pure Bi_2WO_6 presents photo-absorption only from ultraviolet (UV) to visible light regions shorter than 450 nm [20]. The high recombination of its photo-generated electron–hole pairs can limit its photocatalytic activity as well [21]. To enhance its photocatalytic performance, a number of modification methods have been exploited. These methods include doping Bi_2WO_6 with C_60 [22] or with the noble metals Ag [9], CdS quantum dots (QDs) [23], and Eu [12], as well as combining Bi_2WO_6 with narrow band gap semiconductors. Our group has previously reported novel CdS QD-sensitized Bi_2WO_6 heterostructures for degrading methyl orange (MO) dye and phenol [23]. The results indicated that the QD $\text{CdS}/\text{Bi}_2\text{WO}_6$ had a remarkable photocatalytic activity for MO degradation under visible light irradiation. Based on the above mentioned modification methods, we expect that Bi_2WO_6 can also be coupled with the polymeric semiconductor $\text{g-C}_3\text{N}_4$ to expand the research on Bi_2WO_6 and further improve its photocatalytic activity.

Polymeric graphitic carbon nitride ($\text{g-C}_3\text{N}_4$), which has an optical band gap of 2.7 eV, is recognized as the most stable allotrope of

* Corresponding author. Tel.: +86 010 89733200; fax: +86 010 89733200.

E-mail address: gelei08@sina.com (L. Ge).

carbon nitride [24]. Recently, photocatalytic activity of polymeric $\text{g-C}_3\text{N}_4$ for hydrogen or oxygen production from water splitting under visible light illumination was reported by Wang et al. [25] for the first time, and several studies followed [26–30]. Yan et al. [31] synthesized $\text{g-C}_3\text{N}_4$ and used it as a photocatalyst to degrade organic dyes such as MO under visible light irradiation. Very recently, the novel $\text{TaON-g-C}_3\text{N}_4$ and $\text{TiO}_2\text{-g-C}_3\text{N}_4$ composite photocatalysts were prepared and used for the photodegradation of rhodamine B as well as water splitting [32,33]. However, the photocatalytic activities of those composites were found to be low. Therefore, more efficient photocatalytic structures need to be developed.

In the present study, considering the synergic effect between Bi_2WO_6 and polymeric $\text{g-C}_3\text{N}_4$, the novel $\text{g-C}_3\text{N}_4/\text{Bi}_2\text{WO}_6$ heterostructured photocatalysts were prepared for the first time via mixing and heating methods. The aim was to improve further the photocatalytic activity of Bi_2WO_6 . The results demonstrated that compared with pure Bi_2WO_6 and $\text{g-C}_3\text{N}_4$, the $\text{g-C}_3\text{N}_4/\text{Bi}_2\text{WO}_6$ heterojunction photocatalyst had a remarkably enhanced MO photodegradation activity under visible light irradiation. The related properties of the $\text{g-C}_3\text{N}_4/\text{Bi}_2\text{WO}_6$ photocatalysts were characterized and discussed. The possible photodegradation mechanism was also proposed based on energy band positions and photoluminescence (PL) spectra. The novel $\text{g-C}_3\text{N}_4/\text{Bi}_2\text{WO}_6$ hetero-structured photocatalyst may have potential applications in environmental purification.

2. Experimental

2.1. Synthesis of the photocatalyst

All chemicals were reagent grade and used without further purification. Bi_2WO_6 was synthesized by the hydrothermal method. The starting materials, Na_2WO_4 and $\text{Bi}(\text{NO}_3)_3$, were mixed in a 1:2 molar ratio. After deionized water was added, white precipitates immediately appeared, and the mixture was stirred for 1 h to promote further the precipitate reaction. The obtained precipitate was placed in a 100 mL Teflon-lined autoclave, to which water was added to ca. 80% of the capacity. The autoclave was maintained at 170°C for 20 h. The resulting pure Bi_2WO_6 powders were then calcined at 300°C in air for 1 h.

The metal-free $\text{g-C}_3\text{N}_4$ powders were synthesized by heating melamine in a muffle furnace. In a typical synthesis run, 5 g of melamine was placed in a semi-closed alumina crucible with a cover. The crucible was heated to 520°C and held for 2 h at a heating rate of $10^\circ\text{C min}^{-1}$. Further deammoniation treatment was performed at 520°C for 2 h. After the reaction, the alumina crucible was cooled to room temperature. The products were collected and ground into powders.

The $\text{g-C}_3\text{N}_4$ and Bi_2WO_6 powders were then ground together. The resultant samples were collected and calcined at 300°C for 1 h in a muffle furnace. The mechanical mixed $\text{g-C}_3\text{N}_4$ and Bi_2WO_6 powder (70 wt% $\text{g-C}_3\text{N}_4$) without heating treatment was also prepared as a reference. The $\text{g-C}_3\text{N}_4/\text{TaON}$ and $\text{g-C}_3\text{N}_4/\text{TiO}_2$ composite photocatalysts were synthesized according to the literature [32,33] in order to compare photocatalytic performance with the $\text{g-C}_3\text{N}_4/\text{Bi}_2\text{WO}_6$ samples.

2.2. Characterization

The crystal structure of the samples was investigated using X-ray diffraction (XRD; Rigaku D/max 2500 v/pc X-ray diffractometer) with $\text{Cu K}\alpha$ radiation at a scan rate of $0.1^\circ 2\theta \text{ s}^{-1}$. The accelerating voltage and the applied current were 40 kV and 40 mA, respectively. The morphology of the samples was examined by field emission scanning electron microscopy (SEM; FEI Quanta 200F; accelerating

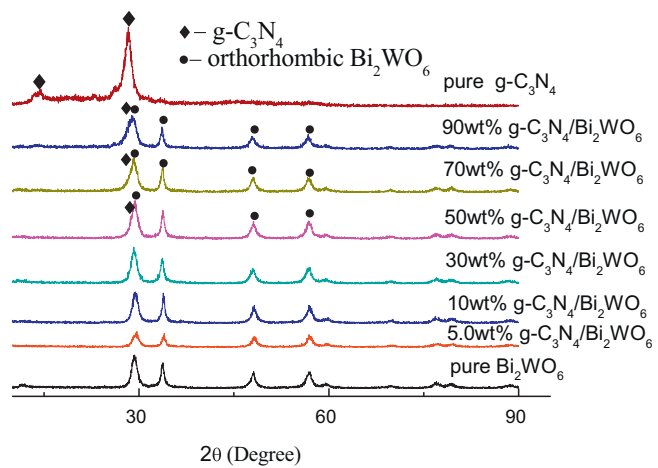


Fig. 1. XRD patterns of pure Bi_2WO_6 and $\text{g-C}_3\text{N}_4$, as well as of the $\text{g-C}_3\text{N}_4/\text{Bi}_2\text{WO}_6$ composite photocatalysts.

voltage = 10 kV) and transmission electron microscopy (TEM; JEOL JEM-2100; accelerating voltage = 200 kV). High-resolution transmission electron microscopy (HR-TEM, FEI Tecnai G² F20) was operated at 200 kV to observe the crystallinity and arrangement of $\text{g-C}_3\text{N}_4$ and Bi_2WO_6 . UV-vis diffuse reflection spectroscopy (DRS) was performed on a Shimadzu UV-3100 spectrophotometer using BaSO_4 as the reference. The PL spectra of the photocatalysts were detected using a Varian Cary Eclipse spectrometer.

2.3. Photocatalytic activity

The photocatalytic activities of the $\text{g-C}_3\text{N}_4/\text{Bi}_2\text{WO}_6$ composite samples were evaluated via the photocatalytic degradation of MO in an aqueous solution under visible light irradiation. A 500 W Xe lamp with a 420 nm cutoff filter provided visible light irradiation. In each experiment, 0.15 g of photocatalyst was mixed with a 50 mL MO solution (10 mg L^{-1}). Prior to irradiation, the suspensions were magnetically stirred in the dark for 30 min to achieve a saturated MO absorption onto the catalyst. At irradiation time intervals of 0.5 h, the suspensions were collected and centrifuged (5000 rpm, 10 min) to remove the photocatalyst particles. The MO concentrations were monitored at 505 nm during the photodegradation process using a UV-vis spectrophotometer (Japan Shimadzu UV-vis 1700).

3. Results and discussion

3.1. Characterization of the $\text{g-C}_3\text{N}_4/\text{Bi}_2\text{WO}_6$ samples

The powder XRD patterns of the as-prepared $\text{g-C}_3\text{N}_4/\text{Bi}_2\text{WO}_6$ composite samples are shown in Fig. 1. The results showed that the photocatalysts were well crystallized. The XRD peaks of the pure Bi_2WO_6 sample were in good agreement with the orthorhombic phase of Bi_2WO_6 (JCPDS 73-1126). The pure $\text{g-C}_3\text{N}_4$ sample had two distinct peaks at 27.4° and 13.1° , which can be indexed as (002) and (100) diffraction planes (JCPDS 87-1526). For the $\text{g-C}_3\text{N}_4/\text{Bi}_2\text{WO}_6$ composites, only Bi_2WO_6 diffraction peaks were found when the $\text{g-C}_3\text{N}_4$ content was below 50 wt%. The characteristic peaks of Bi_2WO_6 (28.2°) and $\text{g-C}_3\text{N}_4$ (27.4°) were too close to distinguish. Nevertheless, weak diffraction peaks corresponding to $\text{g-C}_3\text{N}_4$ (27.4°) appeared when the $\text{g-C}_3\text{N}_4$ content increased from 50 wt% to 90 wt%. Therefore, the $\text{g-C}_3\text{N}_4/\text{Bi}_2\text{WO}_6$ samples had two phases: $\text{g-C}_3\text{N}_4$ and Bi_2WO_6 .

The morphology and microstructure of the $\text{g-C}_3\text{N}_4/\text{Bi}_2\text{WO}_6$ composite samples were revealed by SEM, TEM and HR-TEM. Fig. 2

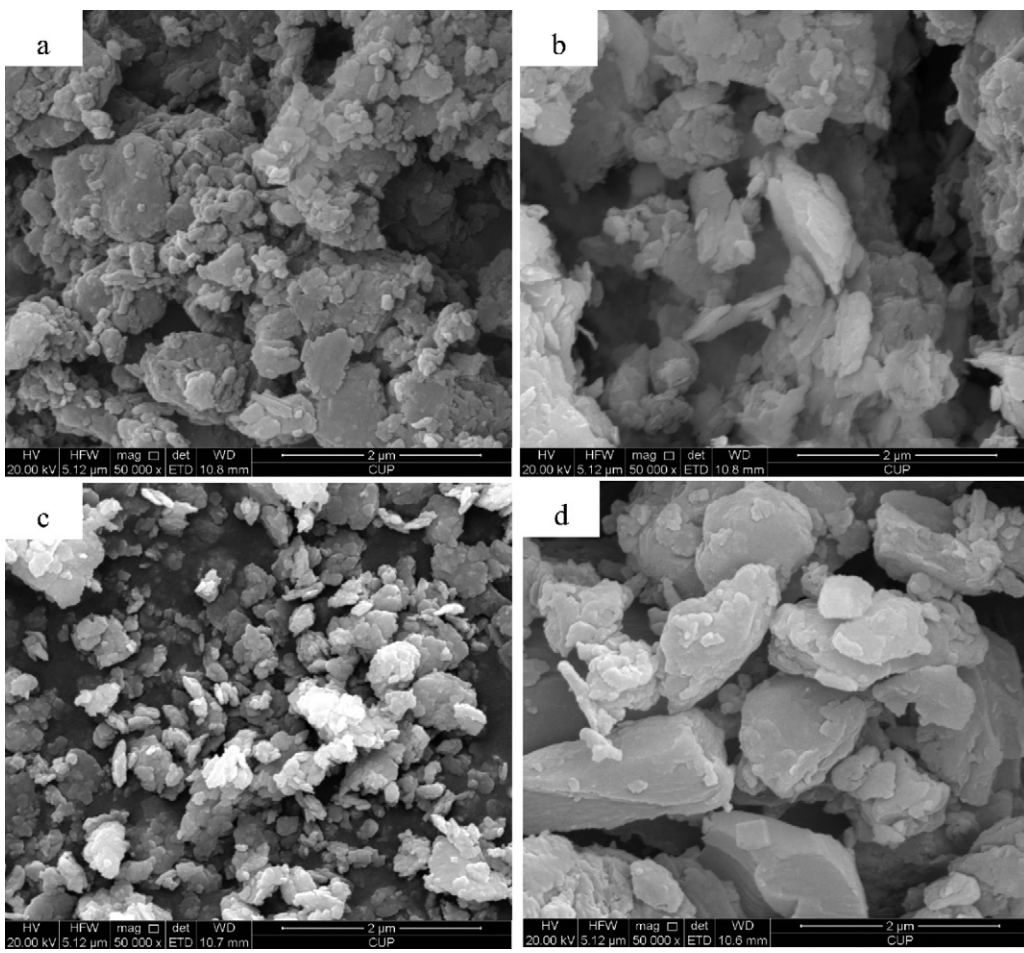


Fig. 2. SEM micrographs of the samples. (a) Pure Bi_2WO_6 . (b) 50 wt% $\text{g-C}_3\text{N}_4$ - Bi_2WO_6 . (c) 70 wt% $\text{g-C}_3\text{N}_4$ - Bi_2WO_6 . (d) Pure $\text{g-C}_3\text{N}_4$.

shows the SEM micrographs of the as-prepared samples with different $\text{g-C}_3\text{N}_4$ doping amount. The pure Bi_2WO_6 samples appeared to have aggregated particles, which contained many smaller Bi_2WO_6 crystals. After introducing $\text{g-C}_3\text{N}_4$, the $\text{g-C}_3\text{N}_4$ / Bi_2WO_6 composite samples showed agglomeration structures, which were similar with pure Bi_2WO_6 . Fig. 2d shows the morphologies of the pure $\text{g-C}_3\text{N}_4$ samples, where even larger particles (diameters of 1000–2000 nm) are observed. Fig. 3a shows the microstructures of the $\text{g-C}_3\text{N}_4$ / Bi_2WO_6 samples via TEM, where $\text{g-C}_3\text{N}_4$ / Bi_2WO_6 is found to consist of irregular 10–30 nm particles. Polycrystalline rings resulting from crystalline particles with the preferred orientation were obtained by selected area electron diffraction. Fig. 3b shows the arrangement of the $\text{g-C}_3\text{N}_4$ and Bi_2WO_6 particles via HR-TEM, where Bi_2WO_6 and $\text{g-C}_3\text{N}_4$ crystallites are seen as having various orientations and lattice spacings. By carefully measuring the lattice parameters using a DigitalMicrograph and comparing with the data in JCPDS, three different kinds of lattice fringes were clearly observed. One fringe with $d = 0.336 \text{ nm}$ matched the (0 0 2) crystallographic plane of $\text{g-C}_3\text{N}_4$ (JCPDS 87-1526). The lattice spaces of the Bi_2WO_6 crystallites were determined as 0.272 and 0.315 nm, belonging to the (0 2 0) and (1 1 3) crystallographic planes of orthorhombic Bi_2WO_6 (JCPDS 73-1126). After heating at 300 °C, obvious interfaces between $\text{g-C}_3\text{N}_4$ and Bi_2WO_6 nanoparticles were observed. This finding suggested that the hetero-junction structure indeed formed from these two materials, and was confirmed by the HRTEM analysis.

The optical absorption of the as-prepared $\text{g-C}_3\text{N}_4$ / Bi_2WO_6 samples was investigated using a UV-vis spectrometer. Fig. 4 shows that the pure Bi_2WO_6 sample absorbs UV to visible lights,

which signifies its visible-light-induced photocatalytic activity. Compared with the pure Bi_2WO_6 sample, the absorption of the $\text{g-C}_3\text{N}_4$ / Bi_2WO_6 composite samples within the visible light range apparently increased and a red shift appeared upon the addition of $\text{g-C}_3\text{N}_4$ powder. These results are attributed to the interaction between $\text{g-C}_3\text{N}_4$ and Bi_2WO_6 in the composite samples. The absorption intensity of the as-prepared samples also strengthened with increased $\text{g-C}_3\text{N}_4$ amount (from 50% to 70%). The wavelength threshold was determined by elongating the baseline and the steepest tangent of the UV-vis spectra (the wavelength of the intersection was λ_g). The absorption edge of the pure Bi_2WO_6 sample was estimated at 460 nm corresponding to the band gap of 2.70 eV. The UV-vis diffuse reflectance spectra of pure $\text{g-C}_3\text{N}_4$ was also investigated, which had wavelength threshold of 461 nm, corresponding to the band gap of 2.69 eV. The wavelength thresholds of the $\text{g-C}_3\text{N}_4$ / Bi_2WO_6 composite samples were 480 nm for 50 wt% $\text{g-C}_3\text{N}_4$ / Bi_2WO_6 and 530 nm for 70 wt% $\text{g-C}_3\text{N}_4$ / Bi_2WO_6 . The enhanced light absorption of the composite samples led to the production of more electron–hole pairs under the same visible light irradiation, which subsequently results in a higher photocatalytic activity.

3.2. Photocatalytic activity of the samples

To study the photocatalytic activity, the MO molecule (major absorption band at 505 nm) was used as the representative dye for the photo-oxidation reaction. Fig. 5 shows the photocatalytic activities of the $\text{g-C}_3\text{N}_4$ / Bi_2WO_6 composite samples with different $\text{g-C}_3\text{N}_4$ concentrations under visible light irradiation ($\lambda > 420 \text{ nm}$).

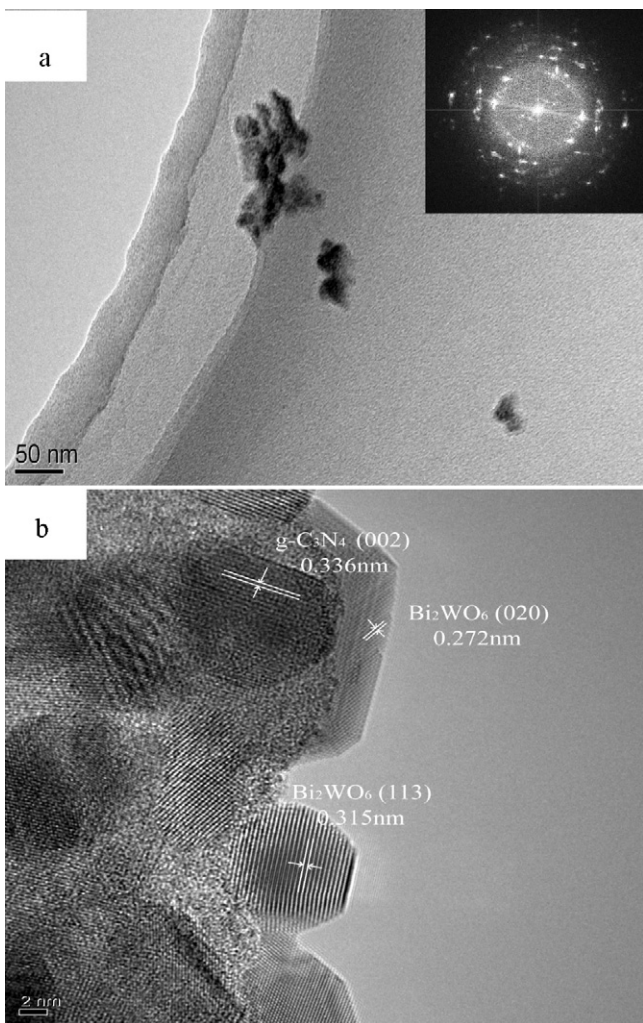


Fig. 3. TEM and HR-TEM images of the samples. (a) TEM micrographs of $\text{g-C}_3\text{N}_4$ - Bi_2WO_6 . (b) HR-TEM images of $\text{g-C}_3\text{N}_4$ - Bi_2WO_6 showing the arrangement of $\text{g-C}_3\text{N}_4$ and Bi_2WO_6 crystallites.

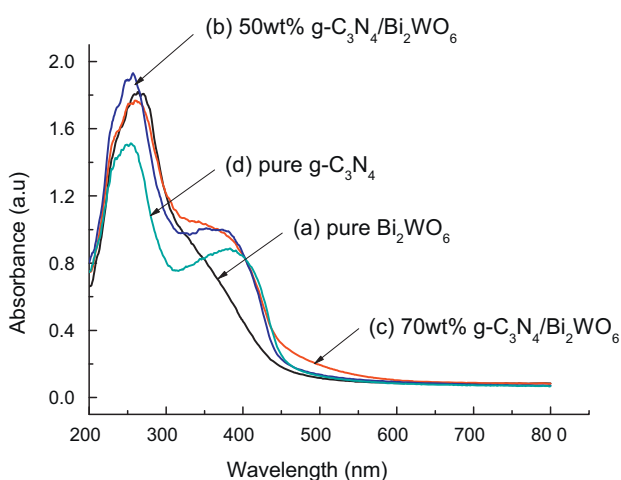


Fig. 4. UV-vis diffuse reflectance spectra of the as-prepared samples. (a) Pure Bi_2WO_6 . (b) 50 wt% $\text{g-C}_3\text{N}_4$ - Bi_2WO_6 . (c) 70 wt% $\text{g-C}_3\text{N}_4$ - Bi_2WO_6 .

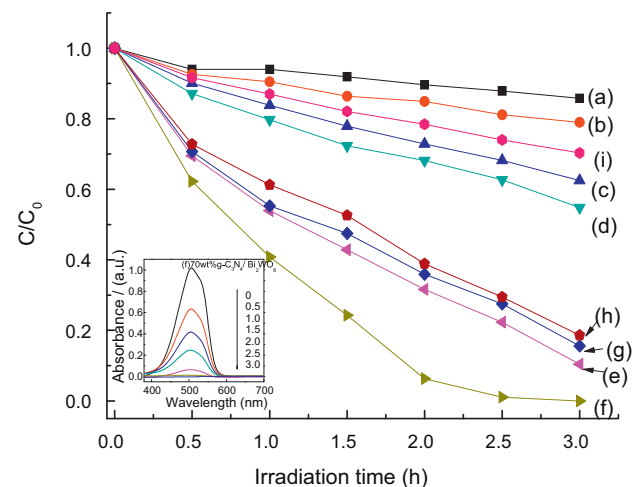


Fig. 5. Degradation rates of methyl orange under visible light irradiation using (a) pure Bi_2WO_6 , (h) pure $\text{g-C}_3\text{N}_4$, as well as $\text{g-C}_3\text{N}_4$ / Bi_2WO_6 with different $\text{g-C}_3\text{N}_4$ concentrations of (b) 5.0 wt%, (c) 10.0 wt%, (d) 30 wt%, (e) 50 wt%, (f) 70 wt%, and (g) 90 wt%.

MO concentration very gradually decreased in the presence of pure Bi_2WO_6 under visible light. Only 14.2% MO was photodegraded after irradiation for 3 h. However, the photocatalytic performance was significantly enhanced after modification by polymeric $\text{g-C}_3\text{N}_4$. When the $\text{g-C}_3\text{N}_4$ amount was 70 wt% of the total catalyst weight, $\text{g-C}_3\text{N}_4$ / Bi_2WO_6 performed best and almost 100% MO was photo-degraded. The inset in Fig. 5 illustrates the variations in MO absorbance around 505 nm using 70 wt% $\text{g-C}_3\text{N}_4$ / Bi_2WO_6 . The absorbance obviously decreased with increased irradiation time. No absorbance peak was observed after irradiation for 3 h, which indicated complete MO decomposition. The photocatalytic results indicated that the doping amount of polymeric $\text{g-C}_3\text{N}_4$ had a significant effect on the catalytic performance of the $\text{g-C}_3\text{N}_4$ / Bi_2WO_6 composite photocatalyst. Fig. 5 shows that the degradation rates were 0.211, 0.376, 0.452, 0.896, 0.999 and 0.844, respectively, for the $\text{g-C}_3\text{N}_4$ / Bi_2WO_6 ratios of 5.0%, 10%, 30%, 50%, 70% and 90%. The rate was 0.814 for pure $\text{g-C}_3\text{N}_4$. At $\text{g-C}_3\text{N}_4$ doping amounts below 70 wt%, the photocatalytic activities improved with increased $\text{g-C}_3\text{N}_4$ doping amount. The degradation ratio of MO increased from 21.1% to 99.9% after irradiation for 3 h. At $\text{g-C}_3\text{N}_4$ loading amounts more than 70 wt%, the photocatalytic activities decreased with increased $\text{g-C}_3\text{N}_4$ amount. The optimal $\text{g-C}_3\text{N}_4$ loading amount on Bi_2WO_6 to achieve an improved photocatalytic activity was determined to be 70 wt%. Hence, the photocatalytic activity of $\text{g-C}_3\text{N}_4$ / Bi_2WO_6 was effectively enhanced compared with that of pure Bi_2WO_6 . This enhancement is attributed to the synergic effect between polymeric $\text{g-C}_3\text{N}_4$ and Bi_2WO_6 , which had an important role in the separation of electron-hole pairs. To confirm the significance of chemical bond formation for the photocatalytic activity of $\text{g-C}_3\text{N}_4$ and Bi_2WO_6 , the photocatalytic degradation experiment over the mechanical mixed powder of C_3N_4 and Bi_2WO_6 (70 wt% $\text{g-C}_3\text{N}_4$ content) was also investigated and illustrated in Fig. 5. The mechanical mixed $\text{g-C}_3\text{N}_4$ and Bi_2WO_6 showed much lower photocatalytic activity than that of 70 wt% $\text{g-C}_3\text{N}_4$ / Bi_2WO_6 composite; the degradation rate was only 0.297 after irradiated for 3 h. The result implied that heating treatment promoted the formation of chemically bonded interfaces between the two materials, and then increased the photocatalytic performance.

To quantitatively investigate the reaction kinetics of the MO degradation, the experimental data were fitted by applying a first-order model as expressed by Eq. (1). This equation is well

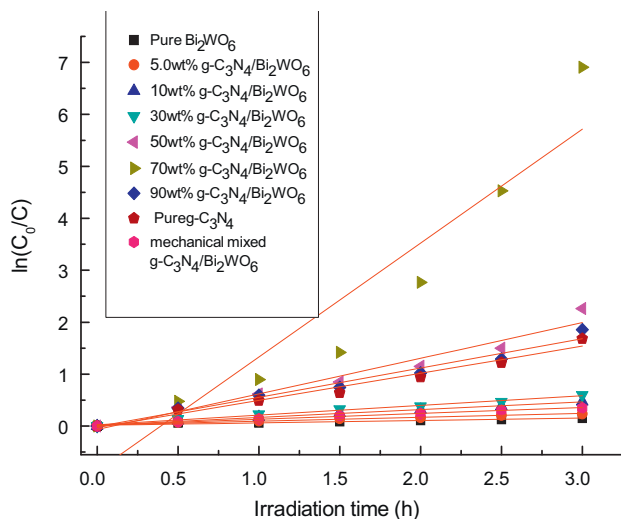


Fig. 6. First-order kinetics plot for the photodegradation of methyl orange by $g\text{-C}_3\text{N}_4/\text{Bi}_2\text{WO}_6$ composite photocatalysts with different $g\text{-C}_3\text{N}_4$ loading amounts.

established for photocatalytic experiments when the pollutant is within the millimolar concentration range.

$$-\ln\left(\frac{C}{C_0}\right) = kt, \quad (1)$$

where C_0 and C are the dye concentrations in solution at times 0 and t , respectively, and k is the apparent first-order rate constant.

Fig. 6 shows the effect of $g\text{-C}_3\text{N}_4$ content on the MO photodegradation rate using $g\text{-C}_3\text{N}_4/\text{Bi}_2\text{WO}_6$. Upon varying the $g\text{-C}_3\text{N}_4$ content within 5.0–90%, the plot of the irradiation time (t) against $\ln(C_0/C)$ was nearly straight line. Fig. 7 shows that the $g\text{-C}_3\text{N}_4$ content greatly influenced the photo-degrading rate (k) of the composite samples. The 70 wt% $g\text{-C}_3\text{N}_4/\text{Bi}_2\text{WO}_6$ exhibited the highest photodegrading efficiency, which was about 47-folds higher than that of pure Bi_2WO_6 . The $g\text{-C}_3\text{N}_4$ content was pivotal for achieving the high photocatalytic activity of the $g\text{-C}_3\text{N}_4/\text{Bi}_2\text{WO}_6$ composite. The suitable $g\text{-C}_3\text{N}_4$ content caused its well dispersion on the Bi_2WO_6 surface, which favored the transfer and separation of the charge carriers. However, at contents higher than 70 wt%, the interfaces and heterojunction structures between the $g\text{-C}_3\text{N}_4$ and Bi_2WO_6 particles decreased. As a result, the interfacial charge transfer was suppressed and the photocatalytic activity was lowered. Therefore, the 70 wt% $g\text{-C}_3\text{N}_4/\text{Bi}_2\text{WO}_6$ was the best performing sample and was selected the cycling study.

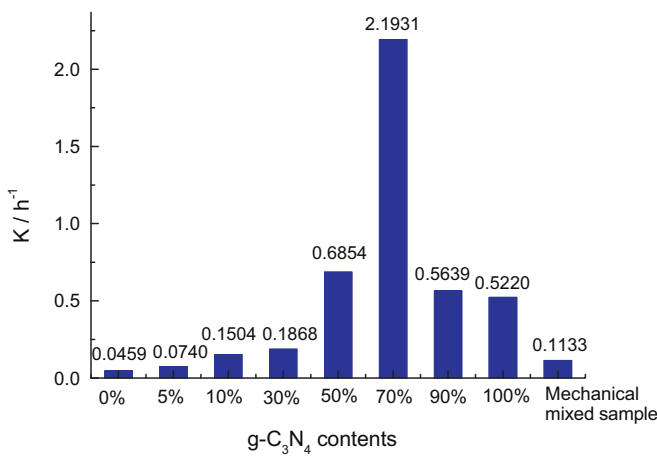


Fig. 7. Photocatalytic degradation rate constant k as a function of $g\text{-C}_3\text{N}_4$ content.

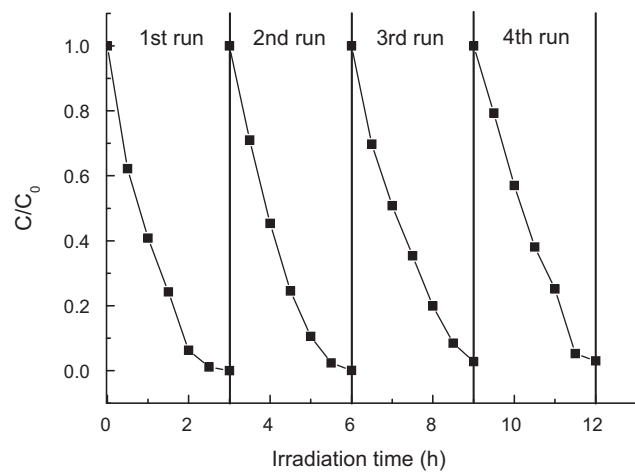


Fig. 8. Cycling runs for the photocatalytic degradation of methyl orange in the presence of 70 wt% $g\text{-C}_3\text{N}_4/\text{Bi}_2\text{WO}_6$ composite under visible light irradiation.

The stability of a photocatalyst is important for its assessment and application. The cycling runs for the photo-oxidation of MO using the 70 wt% $g\text{-C}_3\text{N}_4/\text{Bi}_2\text{WO}_6$ photocatalysts were performed to evaluate its photocatalytic stability. After every 3 h of photodegradation, the separated photocatalysts were washed with deionized water and dried. Fig. 8 shows the decrease in MO in every run. A high MO photodegradation could be maintained after 4 cycling runs and there was no obvious catalyst deactivation. This result confirmed that $g\text{-C}_3\text{N}_4/\text{Bi}_2\text{WO}_6$ was not photo-corroded during the degradation. Variations in the XRD analysis (Fig. 9) also illustrated that the crystal structure of the $g\text{-C}_3\text{N}_4/\text{Bi}_2\text{WO}_6$ photocatalysts did not change after the photocatalytic reaction. Therefore, the $g\text{-C}_3\text{N}_4/\text{Bi}_2\text{WO}_6$ photocatalyst can be concluded as stable given that photo-corrosion did not occur.

For comparison, different composite materials such as $g\text{-C}_3\text{N}_4/\text{TaON}$ and $g\text{-C}_3\text{N}_4/\text{TiO}_2$ were also synthesized and used as photocatalysts in degradation of methyl orange. Fig. 10 shows the degradation rate of methyl orange over different composite photocatalysts under visible light irradiation. As shown in Fig. 10, the degradation rates of methyl orange were 0.999, 0.894, and 0.850 respectively, for the samples of $g\text{-C}_3\text{N}_4/\text{Bi}_2\text{WO}_6$, $g\text{-C}_3\text{N}_4/\text{TaON}$ and

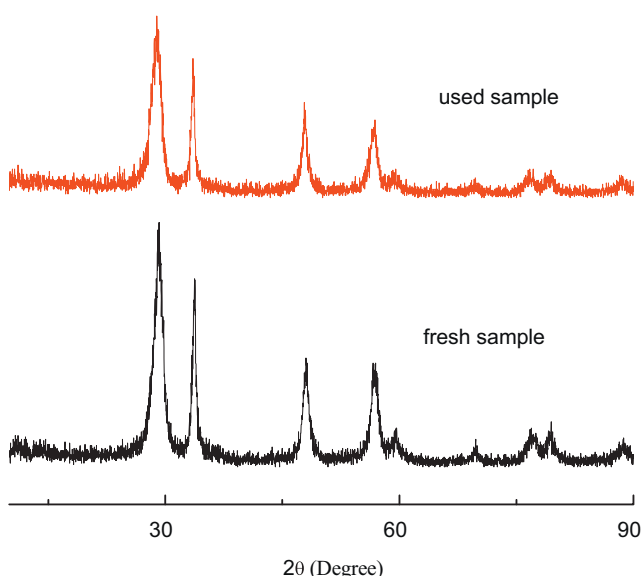


Fig. 9. XRD patterns of 70 wt% $g\text{-C}_3\text{N}_4/\text{Bi}_2\text{WO}_6$ before and after the cycling photocatalytic experiments.

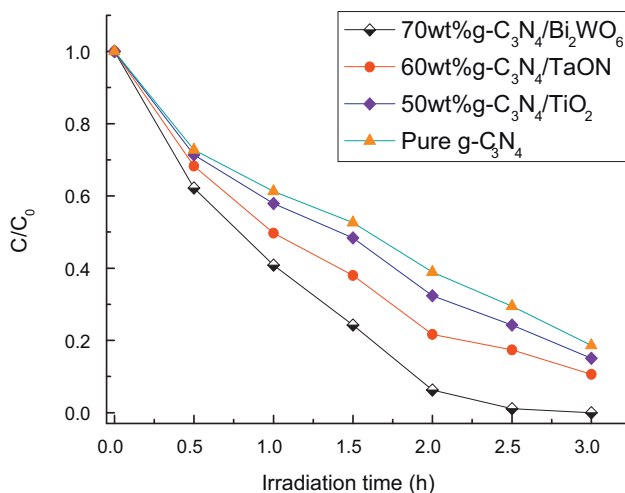


Fig. 10. Comparison of methyl orange degradation over different composite photocatalysts under visible light irradiation: (a) 70 wt% g-C₃N₄/Bi₂WO₆; (b) 60 wt% g-C₃N₄/TaON; (c) 50 wt% g-C₃N₄/TiO₂; (d) Pure g-C₃N₄.

g-C₃N₄/TiO₂. The present experiments clearly indicated that the g-C₃N₄/Bi₂WO₆ was determined as an efficient visible light photocatalyst for the methyl orange degradation.

3.3. Photocatalytic mechanisms

The photocatalytic results have shown the excellent photoactivity of the novel g-C₃N₄/Bi₂WO₆ composite photocatalysts on the degradation of MO. Based on the above data, a possible mechanism for the MO photodegradation using the g-C₃N₄/Bi₂WO₆ heterojunction photocatalyst under visible light irradiation is proposed. The purpose is to guide the further improvement of the photocatalytic performance of the novel composite.

To improve photogenerated carrier separation and enhance the efficiency of interfacial charge transfer, two semiconductors in contact with different conduction band (CB) and valence band (VB) redox energy levels can be used [6]. In the present study, polymeric g-C₃N₄ served as a sensitizer for the visible-light-induced redox process, whereas Bi₂WO₆ was the substrate. The metal-free g-C₃N₄ is a polymeric compound with graphitic planes constructed from tri-s-triazine units connected by planar amino groups, as shown in Fig. 11. The optical band gap of this polymer semiconductor was determined to be 2.7 eV [25]. Therefore, g-C₃N₄ has the photocatalytic ability for water splitting and organic dye degradation under visible light irradiation. On the other hand, the semiconductor Bi₂WO₆ has the ability to absorb visible light, which is attributed

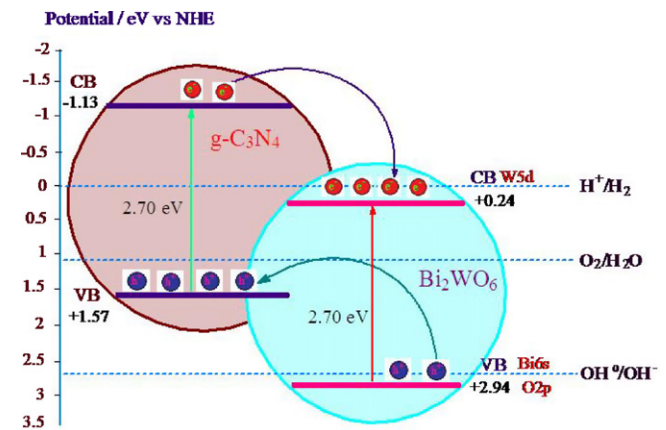


Fig. 12. Diagrams of the energy position and photogenerated electron–hole pair transfers between polymeric g-C₃N₄ and Bi₂WO₆.

to the transition of its electrons from the VB (the hybrid orbital of O_{2p} and Bi_{6s}) to the CB (the W_{5d} orbital) in the catalyst. The band gap of Bi₂WO₆ was determined as 2.7 eV from the DRS spectra, which fairly conforms to a previously reported experimental result [20].

When the polymeric g-C₃N₄ was introduced to Bi₂WO₆, the two types of semiconductor materials closely combined together and the heterojunction structure was formed. Fig. 12 illustrates the flat potentials of the CBs at pH 7 (versus the normal hydrogen electrode) for g-C₃N₄ and Bi₂WO₆ with their band gap energies.

Based on the band gap positions, the CB and VB edge potentials of polymeric g-C₃N₄ were determined at -1.13 and +1.57 eV [25,33], respectively. The CB and VB edge potentials of Bi₂WO₆ were at +0.24 and +2.94 eV, respectively. The CB and VB edge potentials of g-C₃N₄ were more negative than that of Bi₂WO₆. Obviously, the difference between the CB edge potentials of g-C₃N₄ and Bi₂WO₆ allowed the electron transfer from the CB of g-C₃N₄ to that of Bi₂WO₆. When the system was irradiated with visible light, the polymeric g-C₃N₄ (band gap = 2.7 eV) and Bi₂WO₆ (band gap = 2.7 eV) in the composite photocatalyst absorbed photons as well as excited electrons and hole pairs. The process can be described as follows:



The electrons were promoted from the VB to the CB of g-C₃N₄ and Bi₂WO₆, leaving the holes behind. The excited state electrons produced by g-C₃N₄ were then injected into the CB of the coupled Bi₂WO₆. Subsequently, simultaneous holes on the VB of Bi₂WO₆ migrated to that of g-C₃N₄ because of the enjoined electric fields

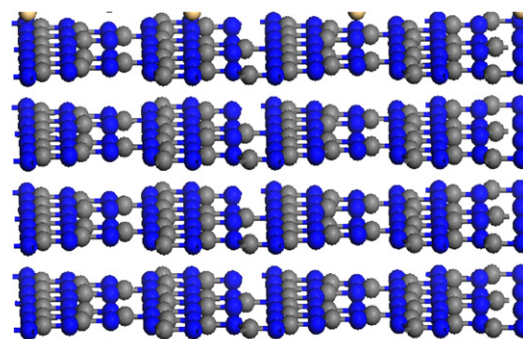
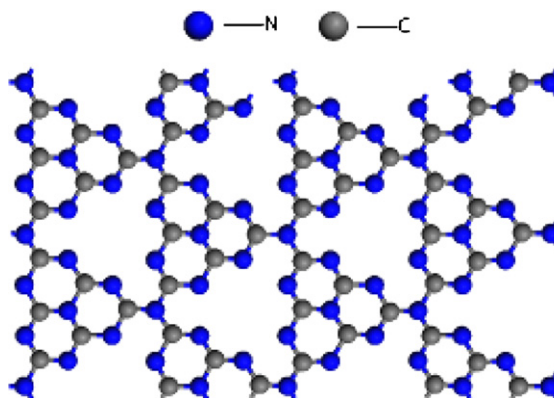


Fig. 11. Schematic diagram of the chemical structure of polymeric g-C₃N₄.

Visible Light Irradiation

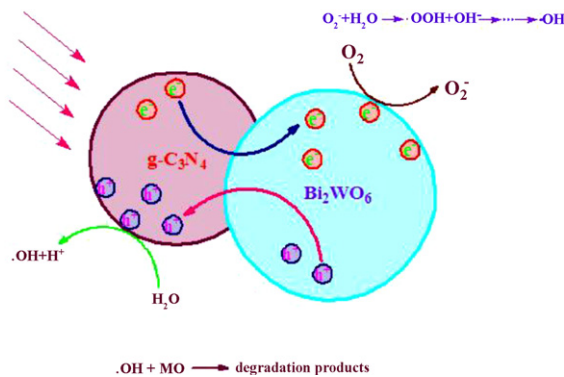
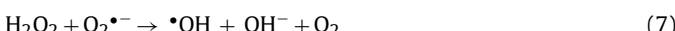
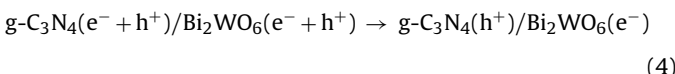
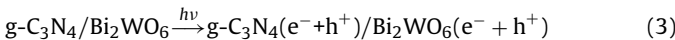


Fig. 13. Redox process of the $\text{g-C}_3\text{N}_4/\text{Bi}_2\text{WO}_6$ composite photocatalysts under visible light irradiation.

of the two materials. The photo-excited electrons were effectively collected by Bi_2WO_6 ; and the holes by $\text{g-C}_3\text{N}_4$, as shown in Fig. 13. Therefore, the recombination process of the electron–hole pairs was hindered, and charge separation as well as stabilization was achieved.

The electrons in Bi_2WO_6 crystals are good reductants that could capture the adsorbed O_2 onto the composite catalyst surface and reduce it to $\text{O}_2^{\bullet-}$. The highly oxidative species $\bullet\text{OH}$ is produced as a consequence of the reduction of oxygen. The photo-generated holes (h^+) in $\text{g-C}_3\text{N}_4$ can also react with H_2O and cause the formation of $\bullet\text{OH}$ groups, leading to a constant stream of the surface $\bullet\text{OH}$ groups. Therefore, the efficient photocatalytic degradation of MO can smoothly proceed. The process is described as follows:



To further investigate the effect of the $\text{g-C}_3\text{N}_4$ modification and confirm the above-proposed mechanism, the PL spectra of $\text{g-C}_3\text{N}_4/\text{Bi}_2\text{WO}_6$ were obtained. PL spectra reveal the migration, transfer, and recombination processes of photo-generated electron–hole pairs in semiconductors. Fig. 14 presents the PL spectra of the $\text{g-C}_3\text{N}_4/\text{Bi}_2\text{WO}_6$ composite photocatalysts at an excitation wavelength of 365 nm. At room temperature, the emission band for pure $\text{g-C}_3\text{N}_4$ was centered at 440 nm, which was attributed to the radiative recombination process of self-trapped excitations. The positions of the $\text{g-C}_3\text{N}_4/\text{Bi}_2\text{WO}_6$ emission peaks were similar with pure $\text{g-C}_3\text{N}_4$. However, the emission intensity of the $\text{g-C}_3\text{N}_4/\text{Bi}_2\text{WO}_6$ composite photocatalysts significantly decreased, with the 70 wt% $\text{g-C}_3\text{N}_4/\text{Bi}_2\text{WO}_6$ sample having the weakest intensity. This result clearly indicated that the recombination of photo-generated charge carriers was inhibited in the composite semiconductors. The PL results conform to the discussion on the charge carrier separation and photocatalytic experiments. Overall, the $\text{g-C}_3\text{N}_4/\text{Bi}_2\text{WO}_6$ heterojunction photocatalysts have very promising applications in the field of environmental purification.

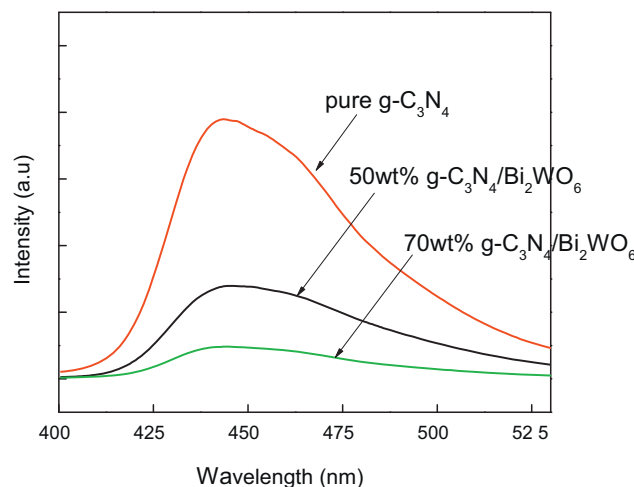


Fig. 14. Photoluminescence spectra of the $\text{g-C}_3\text{N}_4/\text{Bi}_2\text{WO}_6$ composite photocatalysts.

4. Conclusions

Novel visible-light-induced $\text{g-C}_3\text{N}_4/\text{Bi}_2\text{WO}_6$ composite photocatalysts were synthesized by introducing polymeric $\text{g-C}_3\text{N}_4$ via a mixing and heating method. The $\text{g-C}_3\text{N}_4/\text{Bi}_2\text{WO}_6$ samples had a red shift and strong absorption in the visible light region and had obviously enhanced photocatalytic activities in MO degradation. The highest degradation efficiency was observed for the 70 wt% $\text{g-C}_3\text{N}_4/\text{Bi}_2\text{WO}_6$ sample. The synergistic effect was explained and a photocatalytic mechanism was proposed as well as discussed based on energy band positions and PL spectra. The novel heterojunction materials, as highly efficient photocatalysts, may have potential applications in pollutant removal.

Acknowledgments

This work was financially supported by the National Science Foundation of China (Grant no. 21003157), Beijing Nova Program (Grant no. 2008B76), Key Project of Chinese Ministry of Education (Grant no. 108024) and Doctor Foundation of Chinese Ministry of Education (Grant no. 200804251014). We thank the Microstructure Laboratory for Energy Materials and Prof. Lishan Cui for the support of TEM and SEM testing.

References

- [1] M. Shang, W.Z. Wang, S.M. Sun, J. Ren, L. Zhou, L. Zhang, *J. Phys. Chem. C* 113 (2009) 20228–20233.
- [2] R. Asahi, T. Morikawa, T. Ohwaki, K. Aoki, Y. Taga, *Science* 293 (2001) 269–272.
- [3] R. Shi, J. Lin, Y.J. Wang, J. Xu, Y.F. Zhu, *J. Phys. Chem. C* 114 (2010) 6472–6477.
- [4] L. Ge, M.X. Xu, H.B. Fang, *Mater. Lett.* 61 (2007) 63–66.
- [5] L. Ge, M.X. Xu, H.B. Fang, *Appl. Surf. Sci.* 253 (2006) 720–725.
- [6] M.C. Long, W.M. Cai, J. Cai, B.X. Zhou, X.Y. Chai, Y.H. Wu, *J. Phys. Chem. B* 110 (2006) 20211–20216.
- [7] A. Kudo, K. Omori, H. Kato, *J. Am. Chem. Soc.* 121 (1999) 11459–11467.
- [8] Y.L. Lee, C.F. Chi, S.Y. Liu, *Chem. Mater.* 22 (2010) 922–927.
- [9] J. Ren, W.Z. Wang, S.M. Sun, *Appl. Catal. B Environ.* 92 (2009) 50–55.
- [10] X.C. Wang, K. Maeda, X.F. Chen, K. Takanabe, K. Domen, Y.D. Hou, X.Z. Fu, M. Antonietti, *J. Am. Chem. Soc.* 131 (2009) 1680–1681.
- [11] Y. Huo, Y. Jin, Y. Zhang, *J. Mol. Catal. A: Chem.* 331 (2010) 15–20.
- [12] Z.J. Zhang, W.Z. Wang, W.Z. Yin, M. Shang, L. Wang, S.M. Sun, *Appl. Catal. B: Environ.* 101 (2010) 68–73.
- [13] J.W. Tang, Z.G. Zou, J.H. Ye, *Catal. Lett.* 92 (2004) 53–56.
- [14] C. Zhang, Y.F. Zhu, *Chem. Mater.* 17 (2005) 3537–3545.
- [15] H.B. Fu, C.S. Pan, W.Q. Yao, Y.F. Zhu, *J. Phys. Chem. B* 109 (2005) 22432–22439.
- [16] H.B. Fu, L.W. Zhang, W.Q. Yao, Y.F. Zhu, *Appl. Catal. B: Environ.* 66 (2006) 100–110.
- [17] S. Mahanty, J. Ghose, *Mater. Lett.* 11 (1991) 254–256.
- [18] G.K. Zhang, F. Lu, M. Li, J.L. Yang, X.Y. Zhang, B.B. Huang, *J. Phys. Chem. Solid* 71 (2010) 579–585.

- [19] S.W. Liu, J.G. Yu, *J. Solid. State. Chem.* 181 (2008) 1048–1055.
- [20] Z.J. Zhang, W.Z. Wang, M. Shang, W.Z. Yin, *J. Hazard. Mater.* 177 (2010) 1013–1018.
- [21] L. Jiang, L.Z. Wang, J.L. Zhang, *Chem. Commun.* 46 (2010) 8067–8069.
- [22] S.B. Zhu, T.G. Xu, H.B. Fu, J.C. Zhao, Y.F. Zhu, *Environ. Sci. Technol.* 41 (2007) 6234–6239.
- [23] L. Ge, J. Liu, *Appl. Catal. B: Environ.* 105 (2011) 289–297.
- [24] A. Thomas, A. Fischer, F. Goettmann, M. Antonietti, J.O. Muller, R. Schlogl, J.M. Carlsson, *J. Chem. Mater.* 18 (2008) 4893–4908.
- [25] X.C. Wang, K. Maeda, A. Thomas, K. Takanabe, G. Xin, J.M. Carlsson, K. Domen, M. Antonietti, *Nat. Mater.* 8 (2009) 76–80.
- [26] X.F. Chen, J.S. Zhang, X.Z. Fu, M. Antonietti, X.C. Wang, *J. Am. Chem. Soc.* 131 (2009) 11658–11659.
- [27] Y.J. Zhang, T. Mori, J.H. Ye, M. Antonietti, *J. Am. Chem. Soc.* 132 (2010) 6294–6295.
- [28] F.Z. Su, S.C. Mathew, G. Lipner, X.Z. Fu, M. Antonietti, *J. Am. Chem. Soc.* 132 (2010) 16299–16301.
- [29] K. Maeda, X.C. Wang, Y. Nishihara, D.L. Lu, M. Antonietti, K. Domen, *J. Phys. Chem. C* 113 (2010) 4940–4947.
- [30] G. Liu, P. Niu, C.H. Sun, S.C. Smith, Z.G. Chen, G. Lu, H.M. Cheng, *J. Am. Chem. Soc.* 132 (2010) 11642–11648.
- [31] S.C. Yan, Z.S. Li, Z.G. Zou, *Langmuir* 25 (2009) 10397–10401.
- [32] S.C. Yan, S.B. Lv, Z.S. Li, Z.G. Zou, *Dalton Trans.* 39 (2010) 1488–1491.
- [33] H.J. Yan, H.X. Yang, *J. Alloys Compd.* 509 (2011) L26–L29.